LATVIAN JOURNAL OF PHYSICS
AND TECHNICAL SCIENCES
2026, N 2

DOI: 10.2478/lpts-2026-0014

INVESTIGATION OF TEMPERATURE IMPACT ON PHYSICAL PARAMETERS OF AN ELECTRIC DISCHARGE IN ELECTROSTATIC PRECIPITATOR

H. Ait Said [1,2]*, A. Laifaoui [2], K. Barrani [1], N. Hebbar [3],
K. Meziane [4,2], M. Aissou [3,2], H. Nouri [5,2]

[1] Industrial Engineering and Sustainable Development Laboratory,
Ahmed ZABANA University of Relizane,
Relizane 48000, ALGERIA
[2] Electrical Engineering Laboratory,
University of Bejaia,
Bejaia 06000, ALGERIA
[3] Electrical Engineering Department,
University of Ain Temouchent,
Ain Temouchent 46000, ALGERIA
[4] Electrical Engineering Department,
University of Djilali Bounaama Khemis Miliana,
Ain Defla 44000, ALGERIA
[5] Electrical Engineering Department,
University of Setif-1,
Setif, 19000 ALGERIA
*e-mail: hakim.aitsaid@univ-relizane.dz

Research in electric discharge and industrial applications led to the requirement of advanced engineering materials that can withstand various temperatures without significantly affecting their properties. This paper aims to analyse the behaviour of electric discharge in wire-to-plane electrostatic precipitators as a function of temperature. In wire-to-plane electrostatic precipitators at varying temperatures, the physical parameters, including the current-voltage characteristic, onset voltage, corona conductance, electric field, and current density distributions of the discharge DC corona, were experimentally examined, with the corona discharge serving as the ionization source. This project involved the design and construction of an experimental cell to

regulate its internal temperature. The current density and electric field were ascertained using the Tassicker model and a statistical analysis with the regression model validated the current-voltage characteristics. The increase in temperature correlated with a rise in the corona current at the collector plate, while the onset voltage diminished. The applied voltage and temperature significantly influenced the properties of corona current density and the electric field. The temperature for a given atmospheric condition strongly affected the discharge current, according to the experimental results. Changing the values of temperature not only changed the property of the gas but also affected the corona onset conditions and ion mobility.
Keywords: *Corona conductance, current-voltage characteristics, electric discharge, electrostatic precipitator, Tassicker model.*

1. INTRODUCTION

An electric discharge is a phenomenon in which a current flows between two high-potential electrodes in a neutral medium, often air, through the ionization of that medium, resulting in plasma around one electrode, and utilizing the ions produced in plasma processes as charge carriers to the second electrode [1]–[5]. In high-voltage systems, corona can be either positive or negative [6]–[8]. The applications for corona discharge in air treatment and purification include ozone production and electrostatic precipitators for disinfecting water and air [9]–[11]. It is also utilised in electronic devices like photocopiers and laser printers for charging components, as well as for neutralizing static electricity. Scientific applications such as mass spectrometry and surface treatment of materials are further uses [12]–[15].

The physical parameters of an electric discharge encompass electrical variables such as applied voltage, current, electric field, current density, and pulse duration, in addition to other influencing elements like the inter-electrode gap, dielectric medium, and material properties; these parameters dictate the energy and attributes of the discharge [16]–[18]. The corona discharge, in the context of electrostatic precipitators (ESP), refers to a gas discharge phenomenon resulting from the ionization of gas molecules by high-energy electrons within a strong electric field [19], [20]. Electrostatic precipitators effectively eliminate dust by charging the particles through ions generated by the corona discharge electrodes [21]–[23]. The electrically charged particles are then gathered on the collecting plates, to which they are directed by the electric field generated in the interelectrode space due to the voltage applied to the emitter electrodes and collector plates [23], [24]. The formation of corona in the air under atmospheric conditions necessitates a non-uniform electric field, achievable by the utilisation of a small diameter wire electrode paired with a plate or cylinder as the opposing electrode [5], [7], [18].

Industrial electrostatic precipitators (ESPs) are effectively employed to diminish the emissions of smoke, fumes, and dust, so contributing significantly to environmental cleanliness and the attainment of superior air quality, they can eliminate over 99 % of particles from the flue gas [10], [20], [25]. In these systems, particles are charged through ions generated by a DC corona discharge in typical scenarios. The particles move towards the collecting plate as a result of Coulomb forces, while simultaneously being affected by viscous forces from fluid flow and ionic wind [24], [26].

In these systems, understanding the impact of temperature on DC corona discharge behaviour is essential. Certain effects of temperature on DC corona remain inadequately understood and necessitate further exploration to develop realistic and credible models suitable for integration into numerical simulations [23], [27], [28]. The primary aim of this study was to examine the influence of temperature, ranging from 298K to 338K, on the behaviour of positive and negative corona discharge in a wire-to-plane electrostatic precipitator. The analysis and discussion focus on current-voltage curves, corona conductance, onset voltage, electric current density, and electric field.

2. EXPERIMENTAL

2.1. Experimental Apparatus

The experimental method seeks to acquire novel measurements of current density and electric field for both positive and negative DC corona discharge in a laboratory-scaled electrostatic precipitator, as seen in Fig. 1, where the velocity of the particle-free ambient air flow is regulated. Five parallel wires (1) are secured with two insulating supports and positioned equidistantly between two planes (G) at a height of h = 30 mm, with a wire-to-wire spacing of a = 20 mm.

The measurement plane consists of one biased electrode (M) and a circular probe (P). The probe is positioned near the centre of the electrode (M) on the same surface level, with end effects mitigated by the two guard planes (G). All components are constructed from stainless steel and secured with insulating supports. A positive direct voltage from a 0 – ±140 kV source is applied to the wires; a high voltage divider and a DC voltmeter are utilised to measure the applied voltage V(kV) (3). The bias plane (M) is linked to the DC low voltage source, while the collector probe (P) is connected to the digital multimeter (2) through a resistor R_m =150kΩ. The humidity Hr(%) and temperature T(K) monitoring instruments, along with the electrode system, are installed in a 200-liter plexiglass enclosure. The temperature is regulated by the controller (4) and linked online to the low voltage AC source. The air within the plexiglass enclosure is warmed by heating resistors (5). The bigger polarized plate (M) has dimensions of l = 25 mm along the y-axis and L = 150 mm, while the smaller plate (M) measures l = 50 mm along the y-axis and L = 150 mm along the x-axis. The dimensions of the bigger guard plane are 25 mm 150 mm. The electrode system and the temperature measurement devices are situated within a Plexiglas enclosure. The experimental setup is conducted within a sealed system containing purified air. The probe necessitates meticulous assembly. A minor leakage current, about a few milliamperes, may originate from the bias plate (M) or the high voltage cables, hence influencing the current readings. The probe is secured with two insulating plates, and leakage is mitigated through the use of a screen. The leakage current between the corona wires and the probe is directed to the ground by the guard planes (C).

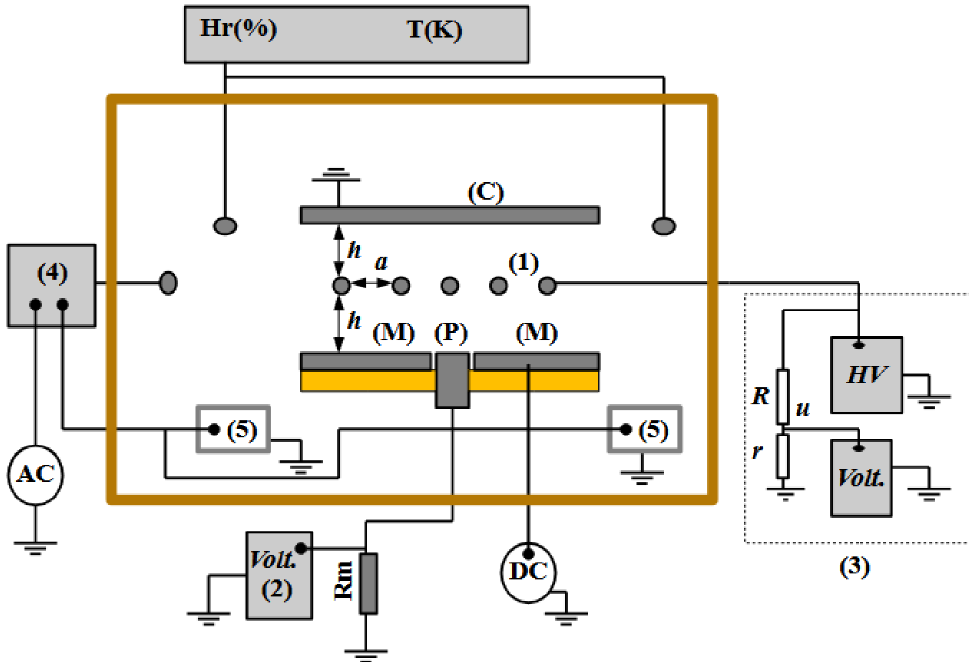

Fig. 1. Experimental model.

2.2. Tassicker Probe Measurement

Figure 2 illustrates the schematic representations of the wires-to-planes ESP utilised in this study. The circular biased probe theory is comprehensively elaborated in references [17], [19], [23], but will be succinctly summarised in this section. The probe collector (P) gathers a current I_0 generated by the corona discharge. The current will be adjusted to (I) when a voltage V_b is applied to the plate (M), generating a bias electric field (E_b). (E_b) is antagonistic to the unknown field (E) at the probe collector's surface (P) when $V_b < 0$, and (E_b) is superimposed on E when $V_b > 0$. An examination of the probe operation conducted by Tassicker [23], [26] provided the ratio of the probe current under influence to the current recorded in the unbiased state. The corona currents (I) under the condition (V_b) and (I_0) under the condition $V_b = 0$ are as follows:

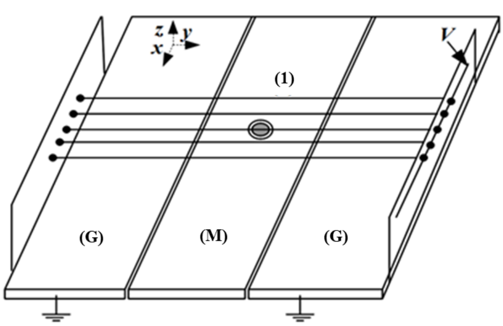

Fig. 2. Geometrical configuration of ESP.

$$I = \mu \times \rho \times \left(\frac{\varphi_{S0} + \varphi_{S1}}{\varepsilon_0} \right), \quad (1)$$

$$I_0 = J_0 \times S = \mu \times \rho \times E \times S = \mu \times \rho \times \frac{\varphi_{S0}}{\varepsilon_0}, \quad (2)$$

$$\frac{I}{I_0} = 1 + \frac{C_0}{\pi \times \varepsilon_0 \times r_m^2} \times \frac{V_b}{E}, \quad (3)$$

$$\frac{I}{I_0} = 1 + Pe \times V_b, \quad (4)$$

$$C_0 = 4r \times \varepsilon_0 \left[1.07944 + 0.5 \times \ln\left(1 + \frac{r}{2g}\right) \right], \quad (5)$$

where μ denotes the positive ion mobility (m²/V·s), ρ represents the space charge density (C/m³), S(m²) signifies the effective surface area of the collector (P), r_m indicates the effective radius, ϕ_{S0} refers to the flux resulting from the unknown electric field E to be measured, and ϕ_{S1} pertains to the flux arising from the biased electric field E_b. C_0 represents the capacitance between the probe collector (P) and the polarized plate (E), where r_m denotes the effective radius of the probe, and ε_0 represents the electrical permittivity of air. The unknown field can then be determined if C_0 is computed. Tassicker employed an analytical expression derived by [17], [19], [23], [26].

$$E = \frac{C_0}{\pi \times \varepsilon_0 \times r_m^2 \times Pe} (kV/m), \quad (6)$$

where Pe is the slope of the linear segment of the experimental feature. The collector probe is utilised to assess the typical current density J(A/m²) when the probe is unbiased, with V_b=0. The subsequent equation delineates the current density [19], [26]:

$$J = \frac{I_0}{\pi \times r_m^2}. \quad (7)$$

3. THEORY OF CURRENT-VOLTAGE CHARACTERISTICS

The corona discharge properties of the electrostatic precipitator are influenced by temperature, as the electric field and ion concentration significantly affect particle charging [23], [27], [29]. In [8], [18], [20], [23], [30], the researchers assert that negative ions are unstable at atmospheric pressures, humidity, and temperatures within the discharge region, where a significant quantity of free electrons is emitted, facilitating the occurrence of sparking even at low applied voltages. The authors of [23] and [27] assert that the ionization rate of gas particles can markedly affect the efficacy of electrostatic precipitation across varying temperatures, and that thermal ionization at elevated temperatures should be considered [31]. The corona discharge is multifaceted phenomena. The authors have formulated a straightforward theoretical equation about the correlation between corona current and applied voltage in a wire-to-cylinder geometric system, alongside a low current empirical law for wire-to-plane arrangement established as follows:

$$I = K \times V \times (V - V_0), \quad (8)$$

where I represents the corona current, V denotes the applied corona voltage, V_0 signifies the corona threshold voltage, and K is a dimensional constant contingent upon the outer cylinder radius, the wire electrode radius, and the mobility of charge carriers in the drift area.

Other authors have documented efforts to derive Townsend's law for the blade-to-plane [17] and wire-to-plane systems [20], [26], [30]. Recent research on the corona current-voltage characteristic has documented efforts to develop a model for Townsend's law that correlates the dimensions of the active electrode radius with the air gap. The structure of cables connecting two planes, as seen in Figure 1, is specifically utilised for the ESPs. This arrangement is the focus of numerous theoretical and experimental investigations. Cooperman [7], [17], [18] was a pioneer in formulating the law governing corona initiation in ESPs. He presents the current-voltage law, equivalent to Townsend's law, in the following manner:

$$I/V = K \times (V - V_0)\,. \tag{9}$$

$$K = \frac{4\pi\varepsilon_0\mu}{h^2 \log(\frac{d}{r_0})}\,. \tag{10}$$

$$for \rightarrow \frac{h}{a} \le 0.6 \Rightarrow d = \frac{4h}{\pi}\,. \tag{11}$$

$$for \rightarrow \frac{h}{a} \ge 2 \Rightarrow d = \frac{a}{\pi} e^{\frac{\pi h}{2a}}\,. \tag{12}$$

Let h represent the space between the wires and the plane, a denote half the wire-to-wire separation, and r_0 signify the wire radius. The impact of humidity on DC corona in electrostatic precipitators (ESPs) is not well understood and necessitates more research. The primary aim of our work is to examine this influence on the behaviour of positive and negative corona discharge in a wire-to-plane arrangement within ESPs.

4. RESULTS AND DISCUSSION

The section discusses the influence of ESP design and temperature on the current-voltage characteristics. The ideal operating conditions for the ESP were established by adjusting the design and operational parameters, including the number of wires and the applied voltage. Prior to starting the ESP, the corona current-voltage characteristics were assessed to estimate the electrical charge of the particles. The current was quantified at the collection plates. All measurements were conducted in a climate-controlled laboratory, where the pressure was sustained at 750 torr, and relative humidity was regulated at 50 % (the physical properties of air are consistently monitored).

4.1. Temperature Effect of Current-Voltage Characteristics

Figure 3 illustrates the current-voltage characteristics for both high voltage polarities. The semi-logarithmic form is utilised to illustrate the initial phase of the corona discharge.

The discharge current rises with the applied voltage until it surpasses the corona onset voltage (V_0), leading to gas breakdown. As anticipated, the corona discharge is initiated at a reduced voltage when the wire diameter diminishes. Moreover, one may also discern the influence of polarity on the current-voltage characteristics. At a specific voltage, the discharge current is greater with negative polarity, attributable to the disparity in the apparent mobility of negative charge carriers relative to positive ones [7], [17], [18], [26]. The ionization process resulting from a collision underpins gas multiplication. The initial Townsend coefficient of a gas refers to the quantity of electron-ion pairs generated by a single electron traversing a unit distance in the direction of the electric field. The outcome primarily relies on the gas type, gas pressure, and electric field strength. The rise in temperature induces a change in the ionization coefficient inside the ionization region and alters the ion mean free path length in the drift region, given a constant potential voltage between the electrodes.

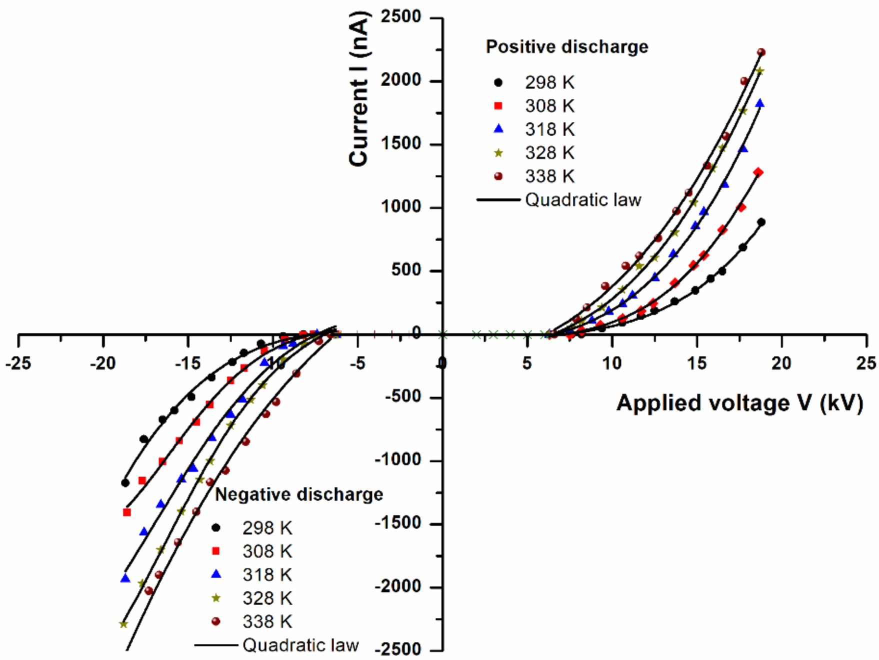

Fig. 3. Current-voltage characteristics of positive and negative DC corona discharge.

4.2. Assessment of the Regression Model Relevance

The estimation of the curve model comprises two elements: the model summary and the parameter estimation provided in Table 1 and Table 2 for positive corona and negative corona. The model summary in these tables presents the regression coefficient (R), the F statistic, which is the ratio of inter-group mean squares to intra-group mean squares, and the significance level (Sig.) indicating the test's significance. Additionally, the parameter estimates detail the coefficients of the quadratic equations (A_0, A_1, and A_2). The F and Sig. columns encapsulate the outcomes of the F test regarding model fit. The significant value of the F statistic is below 0.05 %, indicating that the variation elucidated by each model is not attributable to chance. The R^2 statistics are a superior indicator of the relationship's strength. The quadratic law is a model represented by the equation:

$$I = A_0 + A_1 V + A_2 V^2 \, (\mu A) . \tag{13}$$

The quadratic model can be employed to represent a series that initiates or one that attenuates.

To ensure relevance to the model, the enhancement derived from the independent variable must be substantial, and the residuals between the observed values and the regression should be minimal. This model employs the F-value test for evaluation. The value of F was computed automatically, and the corresponding degree of significance is located in the final column of the model summary [32], [33]. The F value exceeds 650 and is significant at m<0.0005. The likelihood of achieving an F value of this magnitude by random chance is below 0.05 %. Consequently, a statistically significant correlation exists between the dependent variable I(μA) and the independent variable V(kV). Consequently, it can be inferred that the model incorporating a predictor facilitates superior prediction of the variable (I) compared to the model lacking a predictor [23], [32], [33].

Table 1. Model Summary and Parameter Estimates with Dependent Variable: Positive Corona Current I(μA) and Independent Variable: Applied Voltage V(kV)

Temperature T(K)	A_0	A_1	A_2	Adj. R-Square	F-Value	Prob>F
298	360.1026	-95.82583	6.46857	0.99254	799.02864	9.30023E-12
308	535.09118	-143.57485	9.77391	0.99772	2623.20776	2.4869E-14
318	458.50569	-141.10571	9.77391	0.99799	2986.77421	1.29896E-14
328	219.14447	-101.58689	10.71377	0.99878	4905.0556	1.11022E-15
338	-6.92092	-52.68129	9.06751	0.99526	1261.90388	9.57456E-13

Table 2. Model Summary and Parameter Estimates with Dependent Variable: Negative Corona Current I(μA) and Independent Variable: Applied Voltage V(kV)

Temperature T(K)	A_0	A_1	A_2	Adj. R-Square	F-Value	Prob>F
298	504.7009	-135.54389	8.97389	0.9911	668.9252	2.24798E-11
308	203.47691	-91.21907	8.38916	0.99406	1005.03898	2.97273E-12
318	-52.51631	-57.53664	8.69657	0.99106	666.23186	2.29344E-11
328	-98.12695	-55.6723	9.7948	0.99799	2978.86492	1.32117E-14
338	-442.25462	23.11319	7.21658	0.99326	885.43701	5.58253E-12

4.3. Evaluating Data Fit to the Regression Model

Should there be a substantial enhancement in the model, it is imperative to disclose the degree to which the data conform to this model. It is feasible to measure the extent to which the pattern accurately reflects the dispersion of the points in the graph. This information is included in Tables 1 and 2, with index (R) indicating the value of the multiple model correlation. The multiple correlation (R) is regarded as a basic correlation. It signifies the aggregate correlation between all independent variables of the model and the dependent variable. Given that there is a singular independent variable, this coefficient is equivalent in absolute value to the correlation coefficient referenced in [32], [34]–[36]. The multiple correlation coefficient in Tables 1 and 2 exceeds 0.998. This value signifies that the data are highly compatible with the model and is located in the column (R^2). The squared coefficient of correlation yields an R^2 value exceeding 0.991. This illustrates the proportion of variability in the dependent variable (I) elucidated by the regression model.

4.4. Onset Voltage of Electric Discharge

The onset voltage of corona discharge is the applied voltage needed to achieve the critical electric field required for the ionization of air molecules adjacent to the blade surface. The Peek formula correlates the onset voltage with the disruptive critical potential gradient, dependent on inter-electrode distance h, radius of curvature r_c, temperature T, and gas pressure P.

$$V_0 = m_V \times g_0 \times \delta^2 \times r_c \times \left(1 + \frac{0.0308}{\sqrt{\delta \times r_c}}\right) ln\left(\frac{2 \times h}{r_c}\right) \quad (14)$$

$$\delta = \frac{3.92 \times P}{273 + T} \quad (15)$$

The δ parameter is a gas density factor determined by temperature and pressure. Temperature T is expressed in Kelvin (K) and pressure P – in centimetres of mercury (cmHg). At standard temperature and pressure, δ equals 1. The state of the wire is characterised by the factor *mv* irregularity, the curvature radius *rc*, and the inter-electrode gap *h*. Depending on the state of the wire, *mv* ranges from 0.85 to 0.98, with *mv* equalling 1 for ideal smooth wires [16], [23]. The disruptive critical potential gradient *g0* is approximately 30 kV/cm or 27.2 kV/cm for air [16]. Figure 4 illustrates the influence of temperature on corona discharge.

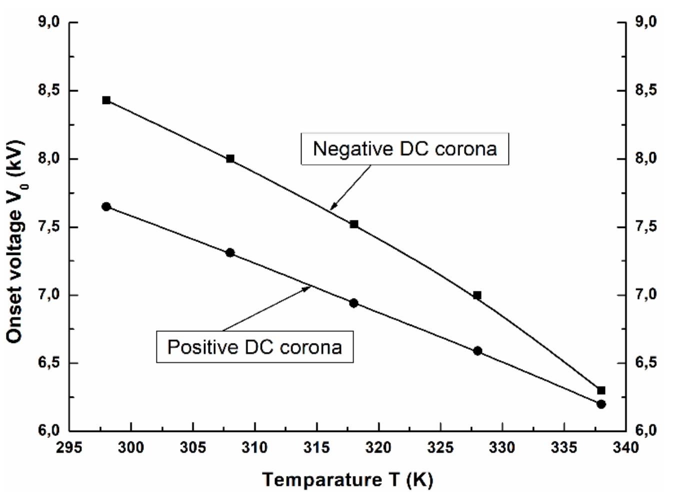

Fig. 4. Variation of corona onset voltage with temperature.

The corona onset voltage diminishes as temperature rises. With additional heat, both the attachment coefficient (η) and the ionization coefficient (α) increase; however, the rise in the attachment coefficient is less pronounced than that of the ionization coefficient. Consequently, the elevation in temperature results in an increase in the effective ionization coefficient (α-η). The aforementioned considerations have led to a reduction in corona onset voltage as temperature rises, resulting in a lower onset voltage at elevated gas temperatures, according to Peek's law.

4.5. Corona Conductance

The importance of the slope of the corona features becomes more evident through the examination of corona conductance trends. The (I/V) = f(V-V_0) graphs serve as an effective assessment of the quadratic law's validity [17], [23]. The slope K and the intercept V_0 with the baseline fully define the glow region of the discharge. The division of the corona current I by V should yield linear relationships, as the current is proportional to (V–V_0). The figure illustrates the positive corona conductance values derived from the data in Fig. 8, whereas the matching negative polarity corona conductance values were computed using the data in Fig. 5, as depicted in Fig. 6. Figure 7 presents a summary of the computed corona conductance slope values. The values acquired at T = 298, 308, 318, 328, and 338 K follow a linear relationship. For extended intervals, there is a reduced departure from the quadratic law. The corona conductance in wire-to-plane for both polarities is approximately 62 % higher. The impact of temperature on conductance is substantial, with the values depicted in Fig. 7 being around 60 % greater.

The geometric factor, or corona conductance G, is contingent upon the mobility of charge carriers μ and the temperature. For the identical geometry, the ratio (K−/K+) also signifies the ratio (μ−/μ+) of the charge carrier mobilities [17], [18]. Nevertheless, we consistently observed in the literature a negligible disparity between the mobilities (μ+) and (μ−), which was less than 10 %. The values of K for the negative corona consistently exceed those of the positive corona at the same temperature. The ratio (K−/K+) = (μ−/μ+) > 1 thus demonstrates that the mobility of negative charge carriers consistently exceeds that of positive charge carriers.

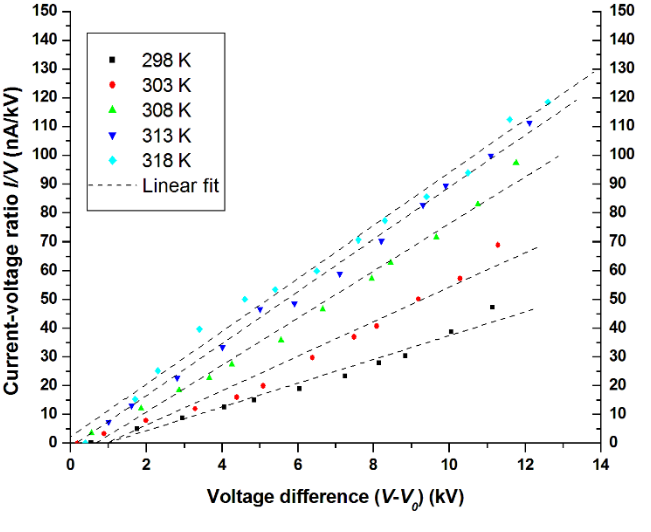

Fig. 5. Positive corona current voltage ratio with various temperatures.

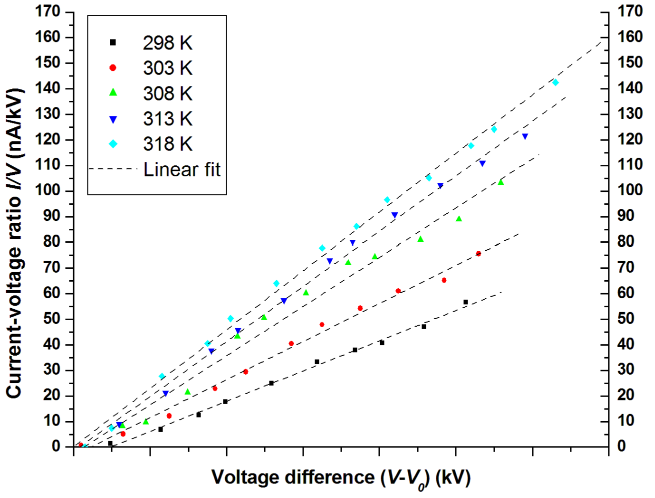

Fig. 6. Negative corona current voltage ratio with various temperatures.

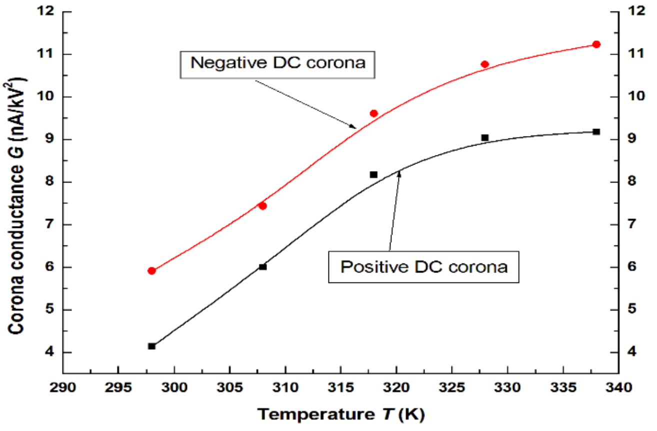

Fig. 7. Corona conductance of both polarities.

4.6. Electric Current Density

The electric current density (Figs. 8 and 9) is defined as the electric current, which is the displacement of a collection of electrical charges, per unit area, where area often refers to the surface layer of an item. Figures 8 and 9 present the experimental results of the measured positive and negative corona current densities at the probe collector, as a function of temperature (T) and varying corona applied voltage (V). The mutual approximation of current density posits that it is directly proportional to the electric field. Figures 8 and 9 illustrate the augmentation in current density corresponding to elevated temperatures at various applied voltages. A few electrons traverse directly to the collector plane, unobstructed by gas molecules, to produce an electron-carrying current when the temperature exceeds 298K.

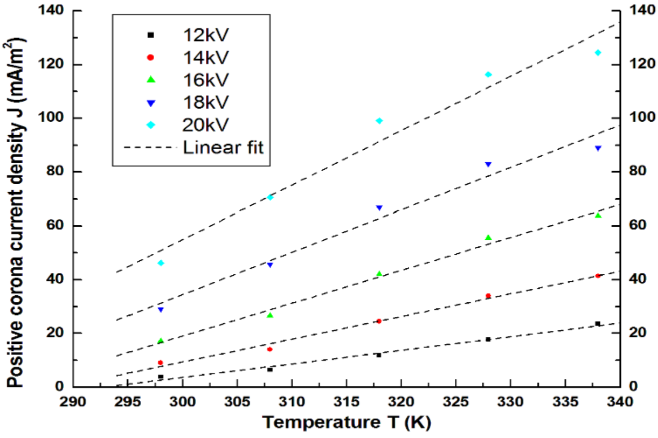

Fig. 8. Current density of positive polarity with various temperatures.

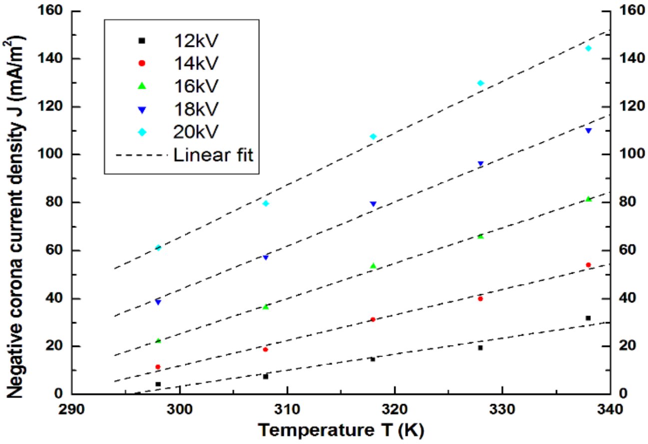

Fig. 9. Current density of negative polarity with various temperatures.

4.7. Electric Field

The influence of temperature on the mean electric field is seen in Figs. 10 and 11. The discharge electric field is elevated with negative polarity, attributable to the disparity in apparent mobility. This study elucidates the mechanism of electric field generation in an electrostatic precipitator (ESP).

In gaseous applications, ESP generates ions using high voltage electrical input. The selection of geometry is predicated on a wire-plane design due to its ease of implementation and adaptability to various physical conditions. The characteristics of the high voltage electrode may affect the threshold voltage of the corona discharge. This work employs stainless steel electrodes because of its robust capacity to withstand mechanical and electrical stresses, coupled with a significant service life.

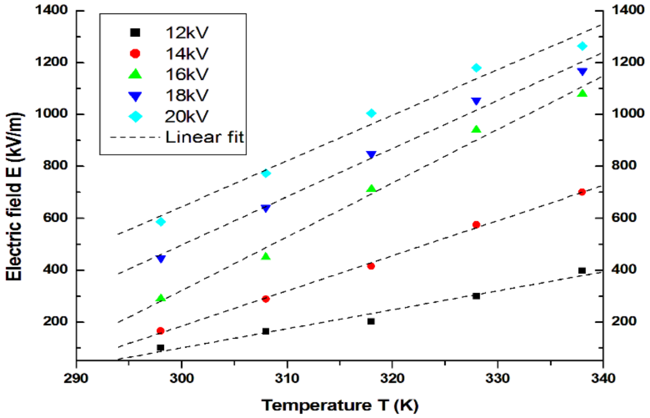

Fig. 10. Electric field of positive polarity with diverse temperatures.

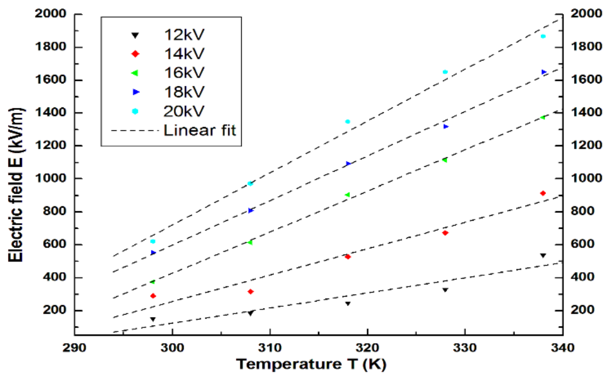

Fig. 11. Electric field of negative polarity with diverse temperatures.

5. CONCLUSION

The study discussed the influence of temperature on the behaviour of direct current corona discharge in a wire-to-plane electrostatic precipitator, encompassing both positive and negative polarities. The voltage-current characteristics in an electrostatic precipitator are crucial for diagnosing electrical issues during its operation. The current-voltage characteristics are readily measurable and furnish most of the necessary information. At a specific voltage, the discharge current is greater with negative polarity, attributable to the disparity in the apparent mobility of negative charge carriers relative to positive ones, and the onset voltage is inversely related to the rise in temperature. The current is altered by a bias field that can either counteract or support the dominant field that has to be measured. This study positions the probe surface perpendicular to the discharge electric field, aligning it with the electrode surface to create an annular gap. The observed mobility rises with elevated temperature. The corona power in an electrostatic precipitator is contingent upon air conditions and the applied voltage.

ACKNOWLEDGEMENT

The authors would like to acknowledge the help and encouragement they have received from colleagues and collaborators during the course of writing the article.

REFERENCES

1. Conesa, A., J., & Sánchez, M. (2018). The current–voltage characteristics of corona discharge in wire to cylinder in parallel electrode arrangement. *IEEE Transactions on Plasma Science*, *46*(8), 3022–3030. https://doi.org/10.1109/TPS.2018.2851285
2. Sakoda, T., Kubo, K., Mizutani, M., Chiba, T., Kasuga, Y., & Fukano, T. (2023). Influence of impulse corona discharge on discharge time lag of a surge arrester with a spark gap. *Journal of Electrostatics*, *121*(1), 103783. https://doi.org/10.1016/j.elstat.2022.103783
3. Fu, H., Xu, W., Li, S., Liu, Z., & Yan, K. (2023). Convective heat transfer enhancement by corona discharge in a wire–cylinder electrostatic precipitator with the water-cooling system. *Journal of Electrostatics*, *125*(5), 103845. https://doi.org/10.1016/j.elstat.2023.103845
4. Suvanjumrat, C., Priyadumkol, J., Khaothong, K., & Chaiworapuek, W. (2025). An empirical investigation into enhancing natural convection heat transfer through corona wind in a needle-to-cylinder configuration, *Case Studies in Thermal Engineering*, *68*(4), 105864. https://doi.org/10.1016/j.csite.2025.105864
5. Moreau, E., Benard, N., Lan-Sun-Luk, J. D., & Chabriat, J. P. (2013). Electrohydrodynamic force produced by a wire-to-cylinder dc corona discharge in air at atmospheric pressure. *Journal of Physics D: Applied Physics*, *46*(47), 475204. https://doi.org/10.1088/0022-3727/46/47/475204
6. Kasdi, A., Chouali, S., Bekakria, A., & Dascalescu, L. (2023). Experimental and numerical modeling of DC corona discharge in wire-cylinder-plane configuration. *Journal of Electrostatics*, *123*(3), 2023, 103814. https://doi.org/10.1016/j.elstat.2023.103814
7. Ait Said, H., Nouri H., & Zebboudj, Y. (2014). Analysis of current-voltage characteristics in the wires-to-planes geometry during corona discharge. *The European Physical Journal Applied Physics*, *67*(3), 30802. https://doi.org/10.1051/epjap/2014140089
8. Aissou, M., Ait Said, H., Nouri, H., & Zebboudj, Y. (2015). Effect of relative humidity on current–voltage characteristics of monopolar DC wire-to-plane system. *Journal of Electrostatics*, *76*(4), 108–114. https://doi.org/10.1016/j.elstat.2015.05.019
9. Yan, X., & Lu, J. (2024). Numerical investigation of the sensible heat storage in novel electrostatic precipitators with liquid-filled collection electrodes. *Applied Thermal Engineering*, *255*(25), 123993. https://doi.org/10.1016/j.applthermaleng.2024.123993
10. Hebbar, N., Aitsaid, H., Aissou, A., Nouri, H., & Zeghloul, T. (2024). Experimental study of the collection efficiency of three configurations of blades-plates-type electrostatic precipitators. *Particulate Science and Technology*, *42*(6), 1020–1030. https://doi.org/10.1080/02726351.2024.2320098
11. Gao, K., Xu, H., Li, J., Wang, C., Dong, B., Chen, C., … & Qian, M. (2025). The influence of gas temperature on ozone generation in atmospheric air dielectric barrier discharge plasma. *Vacuum*, *240*(10), 114587. https://doi.org/10.1016/j.vacuum.2025.114587
12. Hiraoka, K., Shimada, H., Kinoshita, K., Rankin-Turner, S., & Ninomiya, S. (2024). What is the advantage of alternative current (AC) corona discharge for APCI mass spectrometry?, *International Journal of Mass Spectrometry*, *504*(10), 117299. https://doi.org/10.1016/j.ijms.2024.117299

13. Hu, P., Yang, W., Zhang, J., Yu, Z., Zhang, X., Chingin, K., … & Zhang, X. (2025). Rapid evaluation of vegetable oil varieties and geographical origins by ambient corona discharge ionization mass spectrometry. *Food Chemistry*, *464* (6), 141699. https://doi.org/10.1016/j.foodchem.2024.141699
14. Jo, E., Kim, H., Park, Y., J., Park, H., & Lee, M. (2023). Characterization of corona discharge treatment on PTFE surface for TENG applications, *Journal of Electrostatics*, *126*(5), 103865. https://doi.org/10.1016/j.elstat.2023.103865
15. Hassani, F. O., Merbahi, N., Oushabi, A., Elfadili, M. H., Kammouni, A., & Oueldna, N. (2020). Effects of corona discharge treatment on surface and mechanical properties of Aloe Vera fibers. *Materials Today: Proceedings, 24* (Part 1), 46–51. https://doi.org/10.1016/j.matpr.2019.07.527
16. Guo, B. Y., Guo, J., & Yu, A. B. (2014). Simulation of the electric field in wire-plate type electrostatic precipitators, *J. Electrosta.*, *72*(4), 301–310.
17. Kaci, M., Ait Said, H., Laifaoui, A., Aissou, A., Nouri, H., & Zebboudj, Y. (2015). Investigation on the corona discharge in blade-to-plane electrode configuration, *Braz. J. Phys.*, *45*(6), 643–655.
18. Ait Said, H., Aissou, A., Nouri, H., & Zebboudj, Y. (2019). Analysis of the current–voltage characteristic during the corona discharge in wires-to-planes electrostatic precipitator under variable air humidity. *Acta Phys. Pol. A*, *135*(3), 320–325.
19. Nouri, H., & Zebboudj, Y. (2010). Analysis of positive corona in wire-to-plate electrostatic precipitator. *The European Physical Journal Applied Physics, 49*(1), 11001. https://doi.org/10.1051/epjap/2009181
20. Nouri, H., Zouzou, N., Dascalescu, L., & Zebboudj, Y. (2016). Investigation of relative humidity effect on the particles velocity and collection efficiency of laboratory scale electrostatic precipitator. *Process Safety and Environmental Protection*, *104*(7), 225–232. https://doi.org/10.1016/j.psep.2016.09.001
21. Arif, S., Brankena, D. J., Eversona, R. C., Neomagusa, H. W. J. P., Norasb, M. A., le Grangea, L. A., & Arif, A. (2021). An experimentally validated computational model to predict the performance of a single-channel laboratory-scale electrostatic precipitator equipped with spiked and wire discharge electrodes. *Journal of Electrostatics*, *112*(4), 103595. https://doi.org/10.1016/j.elstat.2021.103595
22. Zhou, W., Jiang, R., Sun, Y., Chen, B., & Liu, B. (2021). Study on multi-physical field characteristics of electrostatic precipitator with different collecting electrodes. *Powder Technology*, *381*(6), 412–420. https://doi.org/10.1016/j.powtec. 2020.12.028
23. Ait Said, H., Aissou, M., Laifaoui, A., Hebbar, N., Kaci M., Nouri, H., & Zebboudj, Y. (2022). Experimental Analysis of Corona Current Density Distribution and Electric Field at Variable Temperatures in Electrostatic Precipitator. *Surface Engineering and Applied Electrochemistry*, *58*(4), 339–349. https://doi.org/10.3103/S1068375522040032
24. Nouri, H., Aissou, M., Ait Said, H., & Zebboudj, Y. (2017). Active electrode shape effect on the corona discharge in an electrostatic precipitator. *Environmental Engineering and Management Journal*, *16*(11), 2545–2551. https://doi.org/10.30638/eemj.2017.264
25. Anagnostopoulos, J., & Bergeles, G. (2002). Corona discharge simulation in wire-duct electrostatic precipitator. *Journal of Electrostatics*, *54*(2), 129–147. https://doi.org/10.1016/S0304-3886(01)00172-3
26. Ait Said, H., Nouri, H., & Zebboudj, Y. (2015). Effect of air flow on corona discharge in wire-to-plate electrostatic precipitator. *Journal of Electrostatics*, *73*(1), 19–25. https://doi.org/10.1016/j.elstat.2014.10.004
27. Yan, P., Zheng, C., Zhu, W., Xu, X., Gao, X., Luo, Z., … & Cen, K. (2016). An experimental study on the effects of temperature and pressure on negative corona discharge in high-temperature ESPs. *Applied Energy*, *164*(4), 28–35, https://doi.org/10.1016/j.apenergy.2015.11.040

28. Yang, Z., Li, P., Hu, F., Li, H., Shao, L., & Zheng, C. (2025). Corona discharge and heat transfer coupled to drive the removal of fine particles and simultaneous water recovery from wet flue gas. *Process Safety and Environmental Protection*, *203*(13), 107845. https://doi.org/10.1016/j.psep.2025.107845
29. Syu, J. Y., Huang, S. Y., Cheng, Y. C., Lu, S. H., Wang, C. T., Kao, Y. Y., & Lin, W. Y. (2022). The Applications and Distinctions of Three Different Material Collection Plates in Wet Electrostatic Precipitator. *Aerosol and Air Quality Research*, *22*(10), 220133, https://doi.org/10.4209/aaqr.220133
30. Hamou, N., Aissou, M., & Zebboudj, Y. (2013). Modeling and simulation of the effect of pressure on the corona discharge for wire-plane configuration. *IEEE Transactions on Dielectrics and Electrical Insulation*, *20*(5), 1547–1553. https://doi.org/10.1109/TDEI.2013.6633682
31. Yongmin Shi, Y., Fang, M., Wang, Q., Yan, K., Cen, J., & Luo, Z. (2023). Enhanced high-temperature particle capture through an electrostatic precipitator with assistant electrodes. *Separation and Purification Technology*, *324*(24), 124550. https://doi.org/10.1016/j.seppur.2023.124550
32. Weisberg, S. (2014). *Applied linear regression*. New Jersey: Wiley.
33. Cohen, J. (1988). *Statistical power analysis for the behavioral sciences*. New York: Lawrence Erlbaum Associates.
34. Tenenhaus, M. (2007). *Statistique méthodes pour décrire, expliquer et prévoir*. France: Dunod.
35. Dodge, Y., & Rousson, V. (2004). *Analyse de régression appliquée*. France: Dunod.
36. Johnston, J., & Dinardo, J. (1999). *Méthodes* économétriques. France: Economica.